Macromolecules

ARTICLE

pubs.acs.org/Macromolecules

Structure of Polyelectrolytes with Mixed Monovalent and Divalent Counterions: SAXS Measurements and Poisson−Boltzmann Analysis

Jérôme Combet*,† and Michel Rawiso

Institut Charles Sadron, CNRS-UdS, 23 rue du Loess, BP 84047, 67034 Strasbourg Cedex 2, France

Cyrille Rochas

Centre de Recherches sur les Macromolécules Végétales, CNRS, BP 53, 38041 Grenoble 9, France

Sven Hoffmann

Dubble CRG beamline, European Synchrotron Radiation Facility, 6 rue Jules Horowitz, BP 220, 38043 Grenoble Cedex 9, France

François Boué

Laboratoire Léon Brillouin, CEA-CNRS, CE Saclay, 91191 Gif-sur-Yvette Cedex, France

Supporting Information

ABSTRACT:

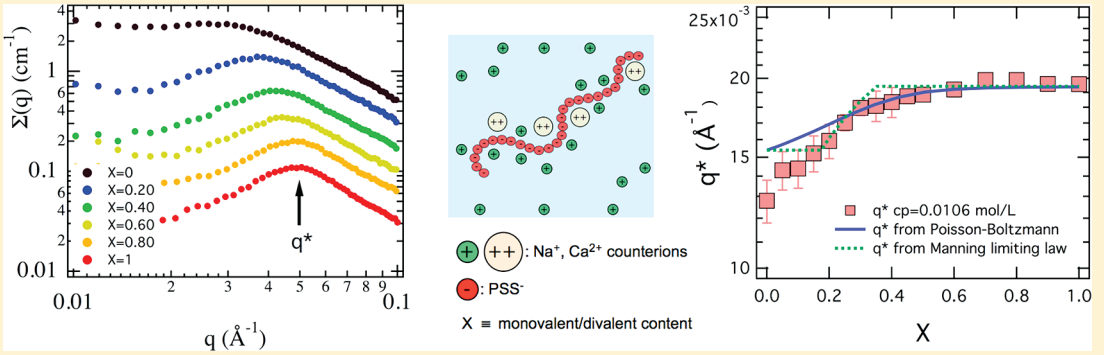

We have studied by small angle X-ray scattering (SAXS) the structure of salt-free polyelectrolytes solutions containing monovalent and divalent counterions. We have considered mixtures of sulfonated polystyrene with monovalent (Na^+) and divalent (Ca^{2+}) counterions and measured the position of the scattering peak, q^*, as a function of the monomer concentration c_p and the monovalent/divalent content. The aim is to understand the variations observed in q^* position when the valence of the counterions is gradually increased. This work is a continuation of a previous study in which first measurements were performed on a rather small number of sodium−PSS/calcium−PSS mixtures. In the present work, we used synchrotron radiation to improve the quality of the data and vary the monovalent/divalent ratio with a much finer step. Indeed this gives new interesting results in the ranges of low and large divalent content. We analyzed SAXS results through the isotropic model and scaling approach description introduced by de Gennes et al. and developed by Dobrynin et al.. In this model, one key parameter is the chemical charge and/or the effective charge fraction f_{eff} of the polyions. Although the chemical charge fraction f of sodium-PSS and calcium-PSS polyelectrolyte is fixed by the synthesis, the effective charge fraction in mixtures varies with the monovalent/divalent ratio. This quantity has been calculated solving the Poisson−Boltzmann equation in the frame of the cell model for various monovalent/divalent contents and different concentrations. Severe deviations are found in the effective charge values of mixtures at finite concentrations compared to the classical Manning−Oosawa prediction (infinite dilution limiting law). We demonstrate that the evolution of q^* is still compatible with the isotropic model and the scaling approach in the low concentration range provided that the divalent content is not too high. In particular, a power law relation $q^* \propto f_{eff}^{\sim 0.3}$ can be found which looks very close to the one observed for weakly charged polyelectrolytes ($q^* \propto f^{2/7}$ in good solvent or $q^* \propto f^{1/3}$ in Θ solvent). Mixtures finally provide a way to adjust the effective charge fraction without changing the chemical nature of the polyions. However this procedure gives improvements to data prediction only in a limited range; it is still not able to fully explain the high concentration range, as well as the high divalent content mixtures. This is certainly due to the fact that the Poisson−Boltzmann theory is not able to take into account local interactions between monomers and divalent counterions, which goes beyond the mean field approach.

Received: September 27, 2010
Revised: February 15, 2011
Published: March 30, 2011

1. INTRODUCTION

Polyelectrolytes (PEL) are a particular class of macromolecules, which dissociate in polar solvent—such as water—into charged macroions and oppositely charged counterions. The solubility in water is a very important characteristic often used in industry in order to take advantage, in water, of the properties of polymer solutions (rheology, emulsion stability, ...). Furthermore, the presence of electrical charges along the chemical sequence brings additional potential: for example, it allows the formation of electrostatic complexes with oppositely charged molecules, colloids or macromolecules and thus offers new possibilities, such as drug design. But even when made of a single species, PEL in water have more complexity, hence more tenability, than neutral polymers in organic solvents: this is due the long-range nature of electrostatic interactions as well as the presence of counterions in the solution. Although a large attention has been paid to this class of material for many years, their properties are not fully understood.[1−6] Among all the parameters driving the properties of PEL solutions (solvent quality, dielectric constant, backbone rigidity, polymer and salt concentrations...),[7] particularly important is the amount of ionized groups on the chain, which controls the polyion charge through a specific mechanism: in the case of highly charged macroions, a fraction of the counterions is condensed around the chains. This phenomenon, often referred as Manning−Oosawa (MO) condensation process,[8,9] reduces the net charge of the macroion (see ref 7 for an overall view) and modifies the electrostatic interactions in the solution. The initial theories of Manning and Oosawa were established for a rodlike macroion. In the case of flexible chains, the problem is more complex: the amount of rigidity is itself due to the polyion charge, so the chain conformation is itself coupled with the electrostatic interactions and the counterion distribution.

The valence of the counterions, or co-ions when multivalent salt is added to the solution, is another key parameter, which can directly affect the average conformation of the chains, their dispersion state and therefore the phase diagram. Depending on the chemical nature of the backbones and the overall rigidity of the chains, different scenarios are expected. In the case of flexible polyacrylate chains for example, specific interactions between divalent cations and the charged backbones (denoted as complex or chemical bonding) lead to a charge neutralization, which modifies the electrostatic/hydrophobic interaction balance. This phenomenon is responsible for a chain collapse and/or the formation of a precipitate.[10] Specific interactions between divalent cations and macroions could also lead to gelation.[11,14] On the opposite boundary of the rigidity range, very stiff polyions (such as double strand DNA) exhibit another behavior: they cannot undergo conformational change so that their interactions are bound to their rod shape. In these systems, the presence of multivalent counterions generate short-range attractive interaction leading for example, to the formation of bundles.[12]

In this paper, we wish to study the effect of the monovalent/divalent counterions ratio on the structure of a highly charged flexible PEL in semidilute salt free aqueous solutions. Because we are only interested in electrostatic effects, our experimental system has been chosen in order to avoid any complexation between macroion and counterions (chemical bonding). We used sulfonated polystyrene (PSS) linear macroions with sodium (Na) and/or calcium (Ca) counterions for which this condition seems to be fulfilled.[13,14] The structure of these solutions has been investigated through small angle X-ray scattering (SAXS). This work is a continuation of a previous study[15] in which scattering measurements were performed on a limited number of sodium−PSS/calcium−PSS mixtures. Small angle X-ray and neutron scattering (SAXS and SANS) provide interesting ways to investigate the structure of the macroions as well as the distribution of counterions around the macroions. The structure functions of PEL solutions display a broad maximum often called "PEL peak". In the case of highly charged PEL such as sulfonated polystyrene, measurements performed in different contrast matching conditions evidence contributions to the peak from both the macroions[16] and the counterions.[15,17−21] This double contribution is a clear demonstration of the strong coupling between the chains and some of the counterion and evidence the presence of a cloud of condensed counterions around the polyions. The origin of this maximum is related to the repulsive interactions between macroions. Its position, q^*, is highly dependent on the monomer concentration c_p[44] and the charge fraction of the macroions; it can be interpreted as related to the mesh size of the transient network describing the structure of PEL semidilute solutions. When increasing the chemical charge fraction f of the polyion, the position of the peak is shifted toward higher q values.[22,59] For higher charge fraction, the position of the PEL peak remains almost independent of f.[23] This has been interpreted as a consequence of the charge renormalization due to the counterion condensation phenomenon: the chemical charge fraction f has then to be replaced by the effective charge fraction f_{eff} which remains constant. Thus, in addition to get insight into the chains organization, a careful investigation of the peak position should allow to probe the complex counterion condensation phenomenon.

In our previous study,[15] we presented an X-ray and neutron small angle scattering study on mixtures of monovalent and divalent counterions in aqueous solutions of polystyrenesulfonate macroions without added salt. The main point was the presence of a scattering peak at a position q^* which scaled in the low concentration regime as $c_p^{1/2}$, with prefactors depending on the monovalent/divalent counterions content. We proposed a very simple model based on MO approach to determine the effective charge fraction of each mixture. Introducing this new charge fraction value f_{eff} in the scaling approach associated with the isotropic phase model of de Gennes et al.[45] (and modified by Dobrynin et al.[46]) allowed the main features of the scattering behavior to be explained. This interpretation was based on the modification of the effective charge fraction according to the monovalent/divalent counterion content. However, the MO model is only valid for rigid infinite chains in the limit of highly diluted samples. In the present work, we first intend to complete our previous measurements by considering a larger set of mixtures, and increasing the scattering pattern quality using the high flux of the synchrotron source at its best. Second, in order to improve the analysis of the SAXS measurements, we intend to determine the effective charge fraction f_{eff} at finite concentration through the resolution of the Poisson−Boltzmann (PB) equation within the cylindrical cell model approximation. We also choose to focus only on the relatively low concentration range for which the PEL peak is always observed. Although the PB approach will not be able to give correct results in the presence of counterion-counterion correlations and/or local monomer/counterions correlations, we expect that this description provides new insight on both the structure of the polyions and the

Table 1. Characteristics of Polystyrene and Sulfonated Polystyrene Samples[a]

	N_n	I	τ_s	τ_w
NaPSS	745	1.04	0.90	0.07
CaPSS	745	1.04	0.90	0.07

[a] N_n is the number-average degree of polymerization of the macroions; I, their polydispersity index. τ_s and τ_w are the degree of sulfonation and the weight fraction of water content of the related dried Na or Ca PEL (obtained from elemental analysis). τ_s is actually the chemical charge fraction f of polyions.

counterion condensation process in PEL solutions with mixed monovalent and divalent counterions.

The paper is organized as follows:

- Section 2 will describe the experimental details such as the characteristics of the investigated PSS samples and the setups of synchrotron radiation experiments
- Section 3 will recall the main aspects of the PB theory and the effective charge fraction determination procedure
- Section 4 will present the SAXS results obtained from several monovalent/divalent contents at different concentrations and the related effective charge obtained from the PB equation
- A discussion will be given in section 5 in the light of the scaling approach associated with the isotropic model.

2. EXPERIMENTAL METHODS

2.1. Materials. The synthesis of the sulfonated polystyrene samples (NaPSS and $Ca_{1/2}$PSS) has already been presented.[15] Polystyrene (PS) chains with a narrow molecular weight distribution were synthesized by anionic polymerization and then sulfonated according to the Makowski et al procedure.[24−27] After neutralization with either sodium hydroxide (NaOH) or calcium hydroxide ($CaOH_2$), NaPSS and $Ca_{1/2}$PSS chains were purified by extended dialysis against pure water (conductivity of the order of 1 μS) and obtained in powder after freeze-drying (note that $Ca_{1/2}$PSS is labeled CaPSS hereafter). Their characterization was carried out by elemental analysis. In this way, the degree of sulfonation τ_s, defined as the ratio of sulfonated monomers to the total number of monomers, and the weight fraction of water content τ_w were determined for each sample. The molecular weights of the parent PS polymer samples (before sulfonation) were characterized by size exclusion chromatography (SEC), using THF as eluent. Table 1 lists the main characteristics of these samples.

Parent solutions of salt-free aqueous solutions of Na−CaPSS mixtures were obtained by dissolving NaPSS and CaPSS powders in ultra pure water (Millipore grade, conductivity <1 μS) in order to get a monomer concentration c_p = 0.34 mol/L. Concentrations and volume fractions are determined from the masses of solute and solvent, by using the tabulated partial molar volumes[28,29] and taking into account the water contents of the various PSS powders. These two solutions were heated until complete dissolution (at 50 °C for 1 h), then let stand for at least 2 days prior to their manipulation. Successive dilutions from these parent solutions were then carried out to obtain other lower concentrations.

Solutions are characterized by their monomer concentration c_p (mol/L), and their fraction of NaPSS macromolecules X, as defined by the molar ratio

$$X = \frac{n_{NaPSS}}{n_{NaPSS} + n_{CaPSS}} = \frac{n_{Na^+}}{n_{Na^+} + 2n_{Ca^{2+}}} \quad (1)$$

where n_{NaPSS} and n_{CaPSS} are the mole number of NaPSS and CaPSS, n_{Na^+} and $n_{Ca^{2+}}$, the mole number of monovalent and divalent counterions. Note that the X parameter defined in this work is equivalent to $\bar{N}_1$ introduced in refs 30 and 31. Six concentrations (c_p = 0.0106, 0.0212, 0.0425, 0.085, 0.17, and 0.34 mol/L), as well as 16 or 17 X values (from X = 0, pure CaPSS to X = 1, pure NaPSS) for each c_p have been investigated. All these solutions are in the semidilute regime and remain absolutely transparent (no visible phase separation).

2.2. SAXS Measurements. Small angle X-ray scattering (SAXS) experiments have been realized at the European Synchrotron Radiation Facility (ESRF, Grenoble, France) on two different CRG beamlines: D2AM (BM2) and DUBBLE (BM26).

D2AM has been used to probe the two lowest concentrations (c_p = 0.0106 and 0.0212 mol/L). Measurements have been performed at λ = 1.033 Å (12 keV) using a single sample to detector distance (d = 2 m). In this configuration, accessible q values ranged from to 0.005 to 0.12 Å^{-1} (q is the magnitude of the scattering vector, defined by the wavelength of the incident beam λ and the scattering angle θ through the relation $q = (4\pi/\lambda)\sin(\theta/2)$.

The four other concentrations (c_p = 0.0425, 0.085, 0.17, and 0.34 mol/L) were investigated on the DUBBLE beamline. This was done at λ = 1.127 Å (11 keV) using mostly one sample to detector distance (d = 8 m) allowing q values from 0.006 to 0.10 Å^{-1} to be investigated. For the highest concentration (c_p = 0.34 mol/L), another sample to detector distance (d = 1.84 m) was necessary to correctly measure the scattering peak, located at larger q. This distance extended the highest accessible q value to 0.55 Å^{-1}.

On both beamlines, the scattered intensity was recorded by a 2-dimensionnal detector. Calibrated mica sheets, one millimeter apart, were used as sample container. Standard ESRF procedures were used for data reduction, and intensity was converted into absolute scale using Lupolen as standard. For the two lowest concentrations, the scattering peak position takes place at a quite low q value and can be hidden by a strong upturn at very low angle. In order to better elucidate the PEL peak, a power law contribution describing the upturn contribution was then subtracted. The error bars also account for the dependence of these positions with the power law estimate.

Under such a procedure, the total differential cross-section per unit volume $\Sigma^{total}(q)$ (cm^{-1}) was obtained for each solution. It is defined as the sum of two terms:

$$\sum^{total}(q) = \sum(q) + \sum^{B}(q) \quad (2)$$

$\Sigma(q)$ is the coherent differential cross-section containing all the information needed to describe the structure of the solution. $\Sigma^B(q)$ is a flat background in the investigated q-range, which has to be removed from $\Sigma^{total}(q)$. For X-ray scattering, this contribution mainly arises from the scattering of the solvent. It can be estimated from the differential cross-section of pure water $\Sigma^{H2O}(q)$ and by taking into account the volume fraction of the solvent in the solution Φ:

$$\sum^{B}(q) = \Phi \sum^{H_2O}(q) \quad (3)$$

For pure NaPSS and CaPSS solutions, we have a multicomponent solute made of large macroions and small counterions, $\Sigma(q)$ actually involves three partial scattering functions:

$$\sum(q) = K_m^2 S_{mm}(q) + K_c^2 S_{cc}(q) + 2K_m K_c S_{mc}(q) \quad (4)$$

In this relation, m refers to macroions and c to counterions; K_m and K_c are their contrast lengths, related to the difference between the scattering length density of the corresponding component and that of pure water. For NaPSS and CaPSS aqueous solutions, neither K_m nor K_c can be neglected: both the macroions and the condensed counterions participate in the scattered intensity and in particular to the PEL peak.

3. THEORETICAL ASPECTS

3.1. Poisson−Boltzmann Equation within the Cylindrical Cell Model. In our previous study,[15] we introduced the effective charge fraction f_{eff} as a function of the monovalent/divalent counterion content X. It was determined from MO condensation criteria[8,9] (limiting law curve in Figure 4). This description is expected to be only valid for very low concentrations certainly out of the experimental concentration range that can be explored by SAXS and SANS. In order to get a better theoretical description of the counterion condensation process, and take into account the finite concentration effect, we intend to use the PB equation in the cylindrical cell model approximation. In the case of highly charged PEL, the MO approach assumes that counterions can be separated in two distinct states: (i) condensed or located near the polyion; (ii) free or scattered in the solution. In the PB theory, making this distinction is inconvenient since the counterion spatial distribution is assumed to vary continuously with the distance from the polyion. However, for highly charged polyions the electrostatic potential is so high that a great fraction of counterions is still located near the polyion even at large dilution. This phenomenon is equivalent to the counterion condensation as defined in MO theory.

Although the PB equation has been widely used in the case of monovalent counterions in order to investigate thermodynamic properties of PEL solutions, there are only few studies concerning monovalent-divalent counterions mixtures.[30−35] These works essentially concern the counterions properties (distribution around the polyions, activity coefficient, osmotic pressure, osmotic coefficient, ...), however the effective charge of the polyions have never been explicitly presented nor calculated. Since it plays a key role in the analysis of the position q^* of the electrostatic peak in small angle scattering experiments, we focus on this particular quantity.

Let us recall the main features of the PB equation and its resolution within the cylindrical cell model for salt free solutions.[36,37] The macroions are treated as sufficiently long rods of radius r_0 so that end chains effects can be neglected. The chains are enclosed in independent cylindrical cells. Each cell contains the right amount of counterions to ensure global charge neutrality. Electrostatic coupling between polyions and counterions of different cells is neglected. The distribution of the polyion charges is replaced by a uniform charge density over the surface of the rod.

The radius of the cell R_c is chosen according to the statistical unit concentration density n_P (m^{-3}), or c_P (mol/L): one unit in a disk of thickness b corresponds to the relation

$$n_P \pi {R_C}^2 b = N_A 1000 c_P \pi {R_C}^2 b = 1 \tag{5}$$

where N_A is the Avogadro's number. In the above description, each monomer (with typical length b) is supposed to carry one negative elementary charge $-e_0$. Counterions (considered as point-like) are described by their cylindrical density $n(r)$ (r is the distance from the cell axis). Since monovalent (valence $Z_1 = 1$) and divalent (valence $Z_2 = 2$) counterions are present in the solution, one has to introduce the monovalent counterion density $n_1(r)$ and the divalent one $n_2(r)$:

$$\begin{aligned} n_1(r) &= Z_1 n_1(R_C) \exp(-Z_1 e_0 \psi(r)/k_B T) \\ n_2(r) &= Z_2 n_2(R_C) \exp(-Z_2 e_0 \psi(r)/k_B T) \end{aligned} \tag{6}$$

$n_1(R_C)$ and $n_2(R_C)$ are the densities of monovalent and divalent counterions at the border of the cell and $\psi(r)$ is the electrostatic potential which is assumed to be zero at the surface of the cell ($r = R_C$), k_B is the Boltzmann's constant and T is the temperature. Both densities are obtained from the solution of the PB equation

$$\left(\frac{d^2}{dr^2} + \frac{1}{r}\frac{d}{dr}\right)\psi(r) = -\frac{e_0}{\varepsilon_0 \varepsilon_r}(Z_1 n_1(R_C) \exp(-Z_1 e_0 \psi(r)/k_B T) + Z_2 n_2(R_C) \exp(-Z_2 e_0 \psi(r)/k_B T)) \tag{7}$$

for $r_0 \le r \le R_C$, where ε_0 and ε_r are the vacuum permittivity and the relative permittivity of the solvent (water).

If we introduce the Bjerrüm length $l_B = {e_0}^2/4\pi\varepsilon_0\varepsilon_r k_B T$ and the Manning charge parameter $\zeta = l_B/b$, the boundary conditions of the PB equation read

$$\left.\frac{d\psi(r)}{dr}\right|_{r=R_C} = 0 \tag{8}$$

and

$$\begin{aligned} \left.\frac{d\psi(r)}{dr}\right|_{r=r_0} &= -2\zeta/k_B T e_0 r_0 = -2 l_B/b k_B T e_0 r_0 \\ &= -e_0/(2\pi b \varepsilon_0 \varepsilon_r r_0) \end{aligned} \tag{9}$$

which reflects the electroneutrality condition in the cell.

Equation 7 was resolved numerically (for fully charged PEL, e.g., $\xi > 1$) for different concentrations using conditions $\psi(R_C) = 0$ and eq 8. $n_2(R_C)$was arbitrary fixed to a given value and $n_1(R_C)$ was adjusted until the condition of eq 9 was fulfilled within 0.01%. In order to validate this resolution procedure, numerical results for pure monovalent counterions systems were compared to the analytical approach: they were found to be identical. In the initial description of the PB equation, r_0 was assumed to be the polyion radius whereas counterion were considered as point-like. As mentioned in ref 38, it is more realistic to consider this radius as the distance of closest approach between the center of mass of the counterion and the axis of the cell. Thus, in the following, r_0 will include a contribution from the diameter of the polyion and from the counterion.

In the case of monovalent counterions, the knowledge of counterion distribution has been used to investigate structural properties as measured by small angle X-ray[39,40] and neutron scattering experiments:[19−21] under particular contrast conditions, it is possible to access to the scattering from the counterions alone, i.e. the partial scattering function S_{CC}. The high q behavior of S_{CC} (typically at $q \gg q^*$, the position of the PEL peak) is intimately related to the form factor of the cloud of counterions, and thus, to the calculated radial counterion distribution:

- For rigid polyions,[39,40] the cylindrical cell model provides a good first approximation although yet it underestimates macroion/counterions correlations: to account for the high q scattering behavior, the r_0 value had to be reduced
- For very flexible polyions, the use of the PB equation is not straightforward.[19−21] The chain conformation is much more complicated, usually far away from fully extended linear configuration, and varies with time. It also depends on concentration since flexible chains gradually shrink with increasing concentration. So, a description in terms of charged rod implies that r_0 as well as the linear charge

density depend on c_p. These effects can introduce large discrepancies between analytical results and molecular dynamics simulations.[41] As mentioned in ref 38, the cylindrical cell model can however apply to PEL systems in which the chains are locally rodlike, provided that their persistence length is much larger that the average distance between neighboring charges. Then, for flexible PEL, such as PSS, the strong local fluctuations of the chain axis may reduce the average effective distance between charges along this axis. Indeed, in refs 19−21, b and r_0 were treated as adjustable parameters to fit the high q region of the scattering curves (i.e., at local scale). A good agreement was obtained provided that b is reduced compared to the geometrical value expected when assuming all-trans conformations.

Therefore, we see from these former experiments that the PB equation provides a reasonable approximation to describe not only rigid but even flexible PEL. However, the choice of the input parameters r_0 and b is not easy. In our case, the situation is even more complicated since divalent counterions may introduce correlations, which are not taken into account in this mean-field approach.[32,33] This effect is certainly more pronounced in the case of high content of divalent counterions. In any case, we expect this description to be more accurate than the simple approach developed in our previous study.[15] Actually, it is the simplest way to take into account the influence of the concentration on the condensation phenomenon and therefore, on the effective charge of the polyions.

3.2. Condensed Counterions and Effective Charge Fraction. In the PB approach, counterions are continuously distributed within the cell (for $r_0 \leq r \leq R_C$). The distinction between *condensed* and *free* counterions requires a precise criterion to be achieved. There are different ways to identify these two populations.[31,42] In this study, we use the method initially proposed in ref 43 and revisited in the frame of the PB theory in ref 42 for monovalent counterion, which we apply for both monovalent $n_1(r)$ and divalent $n_2(r)$ species. In this approach, it is necessary to consider the integrated radial charge distribution per unit length defined for both valences (Z = 1 or 2) as

$$P_Z(r) = b\int_{r_0}^{r} 2\pi r Z n_Z(r)\,\mathrm{d}r \tag{10}$$

This quantity represents the number of elementary charges associated with z-counterions per unit length b enclosed in a cylinder of radius r. According to this definition, the global electroneutrality leads to $P_Z(R_C)$=1 on the border of the cell for pure monovalent (X = 1) and divalent counterions (X = 0) solutions. The evolution of $P_Z(r)$as a function of ln(r), exhibits an inflection point at a radius r equals to the Manning radius R_M.[43] This Manning radius defines the extent of the condensed counterions layer in the cell. From the knowledge of R_M, it is possible to separate condensed and free counterions and determine the effective charge fraction f_{eff}.

In the case of pure monovalent or divalent counterions, the effective charge fraction is given by $f_{\mathrm{eff}} = 1 - P(R_M)$ and equals the prediction b/l_B and $b/2\ l_B$ respectively from MO approach.

For a mixture of monovalent and divalent counterions, due to the numerical procedure, a more complex method has to be applied and is described as follows. An obvious but necessary first step is to check, from $n_1(r)$ and $n_2(r)$ the average concentrations of monovalent $\bar{c}_1$ and divalent $\bar{c}_2$ counterions (in mol/L) within the cell:

$$1000N_A\bar{c}_1 = \frac{2}{{R_C}^2}\int_{r_0}^{R_C} n_1(r)r\,\mathrm{d}r = \frac{P_1(R_C)}{\pi {R_C}^2 b}$$
$$1000N_A\bar{c}_2 = \frac{2}{{R_C}^2}\int_{r_0}^{R_C} n_2(r)r\,\mathrm{d}r = \frac{1}{2}\frac{P_2(R_C)}{\pi {R_C}^2 b} \tag{11}$$

which must be compared to the experimental monomer concentration c_p:

$$c_P = \bar{c}_1 + 2\bar{c}_2 \tag{12}$$

The monovalent content X is now expressed as

$$X = \bar{c}_1/(\bar{c}_1 + 2\bar{c}_2) \tag{13}$$

which is related to the experimental X value (eq 1).

Then, the condensation is examined: we find that $P_1(r)$ and $P_2(r)$ as a function of ln(r) display two different inflection points corresponding to distinct Manning radii R_{M1} and R_{M2} respectively. The average concentration of condensed monovalent ($\bar{c}_1^{cond}$) and divalent ($\bar{c}_2^{cond}$) counterions are then defined by:

$$1000N_A\bar{c}_1^{cond} = \frac{P_1(R_{M1})}{\pi {R_C}^2 b} \quad \text{and} \quad 1000N_A\bar{c}_2^{cond} = \frac{1}{2}\frac{P_2(R_{M2})}{\pi {R_C}^2 b} \tag{14}$$

whereas concentrations of the free counterions are

$$\bar{c}_1^{free} = \bar{c}_1 - \bar{c}_1^{cond} \quad \text{and} \quad \bar{c}_2^{free} = \bar{c}_2 - \bar{c}_2^{cond} \tag{15}$$

Ultimately, the effective charge fraction can be obtained from the relation:

$$f_{eff} = \frac{(\bar{c}_1^{free} + 2\bar{c}_2^{free})}{c_p} \tag{16}$$

At this stage, we can note that there are alternative definitions for the effective charge fraction which could be used to analyze the evolution of the PEL peak position according to the concentration and the monovalent/divalent content.[60] However that described above allows us to describe the main features of the SAXS measurements on PEL with mixed monovalent and divalent counterions.

4. RESULTS

4.1. Evolution of q^* as a Function of Concentration and X. The scattering curves measured at c_p= 0.0212 and 0.17 mol/L for distinct X values are presented in Figure 1 (measurements at c_p= 0.0106, 0.0425, 0.085, and 0.34 mol/L can be found in the Supporting Information). The evolution of q^* as a function of the concentration for different X values is presented in Figure 2. The results agree with the previous less refined measurements[15] and can be summarized as follows:

- In the low concentration range, q^* scales as $q^* \propto {c_p}^{1/2}$ whatever the X value. Changing the X value only changes the prefactor. An accurate determination of the power law exponent gives 0.45 instead of 0.5 previously reported.[15] It must be noticed that our initial work combined X-rays and neutron scattering experiments. We have shown that small differences may be observed in q^* values according to the small angle technique (SAXS or SANS), or more

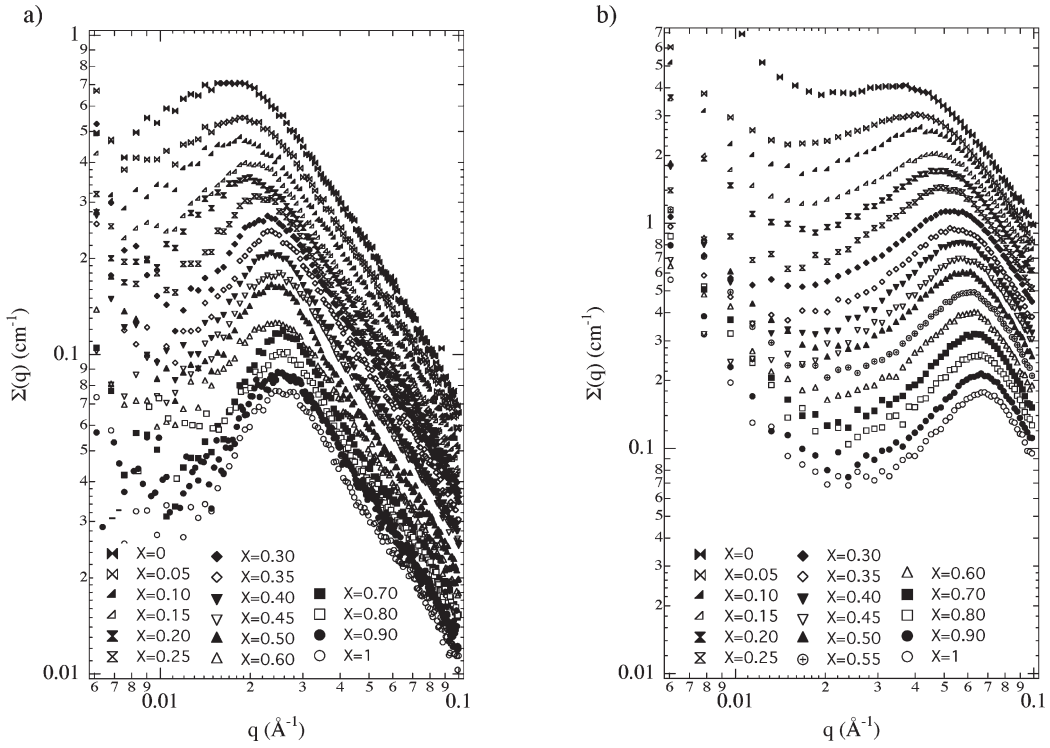

Figure 1. Scattering curves obtained at c_p = 0.0212 mol/L (part a), and c_p = 0.17 mol/L (part b). For sake of clarity, only one point over ten is represented. All the scattering curves have also been vertically shifted, except the one for X = 1.

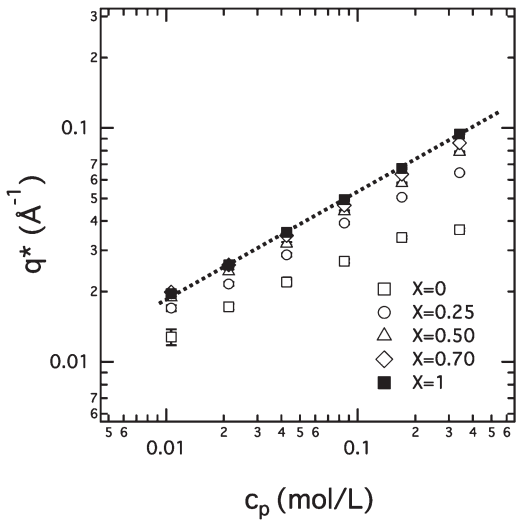

Figure 2. Scattering vector q^* versus monomer concentration c_p for different monovalent/divalent fractions X defined as $(n_{NaPSS})/(n_{NaPSS} + n_{CaPSS}) = (n_{Na^+})/(n_{Na^+} + 2n_{Ca^{2+}})$. For the sake of clarity, only X = 0, 0.25, 0.5, 0.70, and 1 are considered. Dotted line corresponds to a $c_p^{1/2}$ evolution. The total fraction of monovalent counterions (with respect to the total amount of monovalent and divalent counterions) in the solution $(n_{Na^+})/(n_{Na^+} + n_{Ca^{2+}})$ is actually given by $2X/(X + 1)$. For $X \approx 0.18$, we only get 30% of monovalent counterions in the solution; for $X \approx 0.36$, the fraction increases to 53%.

exactly, according to the contrast lengths of the condensed counterions and the polyions. More precisely, a slight decrease in q^* is observed when the scattered intensity from the counterions is predominant. This is the case in the present SAXS investigations. The slight departure from the $c_p^{1/2}$ power law is certainly a simple consequence of the scattering technique

- When the concentration is increased, more important deviations from the $c_p^{1/2}$ scaling law begin to appear. They occur at even lower concentrations for higher divalent counterion ratio (smaller X). For X = 0, the onset of deviation is at c_p = 0.0425 mol/L. For even higher concentrations (above 0.34 mol/L), the PEL peak may even vanish. This critical concentration has not been reached in the measurements reported here.

Better than the variation $q^*(c_p)$ for different X values, the variation $q^*(X)$ at distinct concentrations is certainly a more appropriate representation to highlight subtle variations. It is presented in Figure 3 (with the theoretical approaches addressed in the Discussion) for different concentrations. The main features can be summarized as follows:

- q^* is a monotonic increasing function of X
- For the highest X values (more precisely in between X = 0.7 and 1) and the two smallest concentrations, q^* tends to a plateau. For higher concentrations, this plateau disappears and a weak slope appears for the highest X values. This slope increases with the concentration
- q^* increases more rapidly in the range $0 < X < 0.3-0.4$ for each concentration.

This more complete set of data brings new information compared to our previous study:[15]

- First, new investigated values for $X < 0.2$ do not show any plateau contrary to what expected when combining eq 18 with the simplest theoretical MO prediction of f_{eff} used in ref 15 (dashed line in Figure 3). In this range of X, f_{eff} is supposed to be constant, as seen in the limiting law curve in Figure 4 (see below)

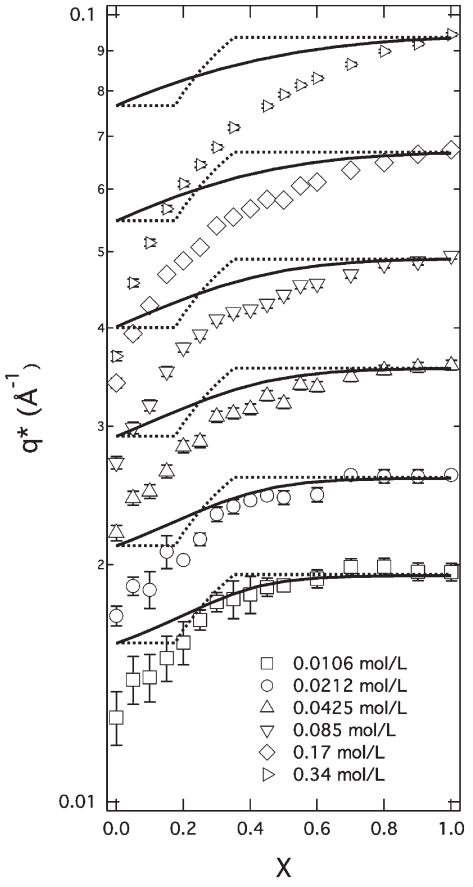

Figure 3. Experimental (symbols) and theoretical (lines) evolutions of q^* as a function of X for different concentrations c_p. The theoretical curves are described in the Discussion: dashed lines correspond to the effective charge evaluated from the MO approach; solid lines, to the effective charge evaluated from the resolution of the PB equation in the cylindrical cell model approximation.

- Second, new investigated values for $X > 0.75$ evidence the second plateau predicted by the MO approach dashed lines in Figure 3, but only for the two lowest concentrations (0.0106 and 0.0212 mol/L). However, the width of the plateau is reduced compared the theoretical expectation (in the range $0.36 < X < 1$).

These two facts could not be detected in our previous study due to the limited investigated X fractions (0, 0.25, 0.5, 0.75, and 1).

4.2. Effective Charge Fraction from the PB Equation. The analysis of the experimental measurements is based on the effective charge prediction. We now consider the variation of f_{eff} according to the models.

The resolution of the PB equation has been achieved for each concentration studied by SAXS. A smaller concentration (10^{-6} mol/L) was also considered in order to check the low concentration behavior. The monomer size b was fixed at 2.52 Å. Calculations have been performed for fully charged macroions. The size of the cylinder r_0 was set to 8 Å. As previously mentioned, it includes the radius of the counterion. The temperature T was 298 K and the corresponding relative permittivity ε_r, 78.3.

The effective charge fraction f_{eff} extracted from the PB equation is presented in Figure 4. It still varies between $b/2l_B$ ($X = 0$) and b/l_B ($X = 1$). But it is now concentration dependent for all intermediate X values. The MO limiting law is also displayed for comparison. Our new numerical computations reproduce this typical behavior for the very diluted solutions (10^{-6} mol/L) only.

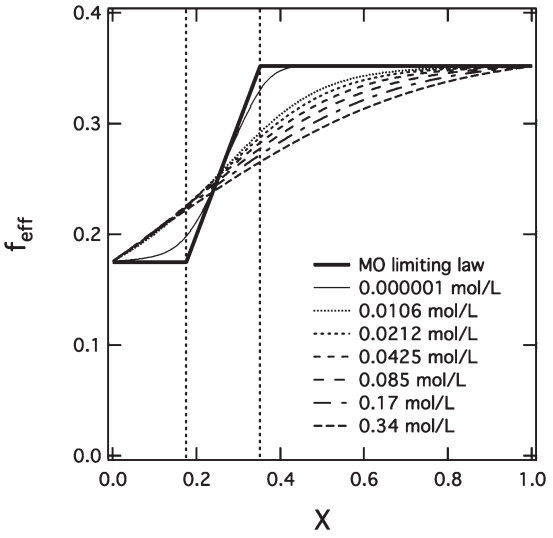

Figure 4. Effective charge fraction f_{eff} as a function of X for different concentrations c_p. The values result from the resolution of the PB equation within the cylindrical cell model. The limiting law considered in ref 15 and corresponding to the MO approach is also indicated. In this approach, the two vertical lines located at $X = b/2l_B \approx 0.18$ and $X = b/l_B \approx 0.36$ separate three different regimes. In between these two lines, f_{eff} is equal to X.

For concentrations higher than 10^{-6} mol/L, specifically those investigated by SAXS, two facts are clear:

- No plateau can be found at very low X values ($X < 0.18$). In this X-range we also note that the values of f_{eff} are nearly identical for all investigated concentrations
- No plateau can be found for $X > 0.36$ (as predicted in the MO description). It vanishes for the investigated SAXS concentration range or, at least, is displaced to higher X range for the lowest concentrations. Actually, a close inspection of the curves rather shows that the tangent even for $X = 1$ displays a weak slope that decreases as the concentration is decreased. The evolution of the effective charge fraction does not show any singularity neither at $X = b/2l_B$ nor at $X = b/l_B$ contrary to what is expected from the MO approach and almost observed for the lowest concentration considered (10^{-6} mol/L).

We present in Figure 5 the variations with X of the fractions of condensed or free counterions (monovalent and divalent) for three distinct concentrations $c_p = 10^{-6}$, 0.0106 and 0.17 mol/L.

For the lowest concentration (10^{-6} mol/L), the simulation, again, leads to results very similar to those of the MO approach (not shown). It shows three different regimes: below $X \approx 0.18$ ($\approx b/2l_B$), all monovalent counterions are free, divalent ones share between free and condensed. The effective charge is constant (limiting law in Figure 4). In between $X \approx b/2l_B$ and $X \approx b/l_B$, all monovalent counterions are free, all divalent are condensed. Changing X in this interval thus introduces a modification of the effective charge fraction. Above $X \approx 0.36$ ($\sim b/l_B$), the monovalent condensed fraction begins to increase

dx.doi.org/10.1021/ma102226v |*Macromolecules* 2011, 44, 3039–3052

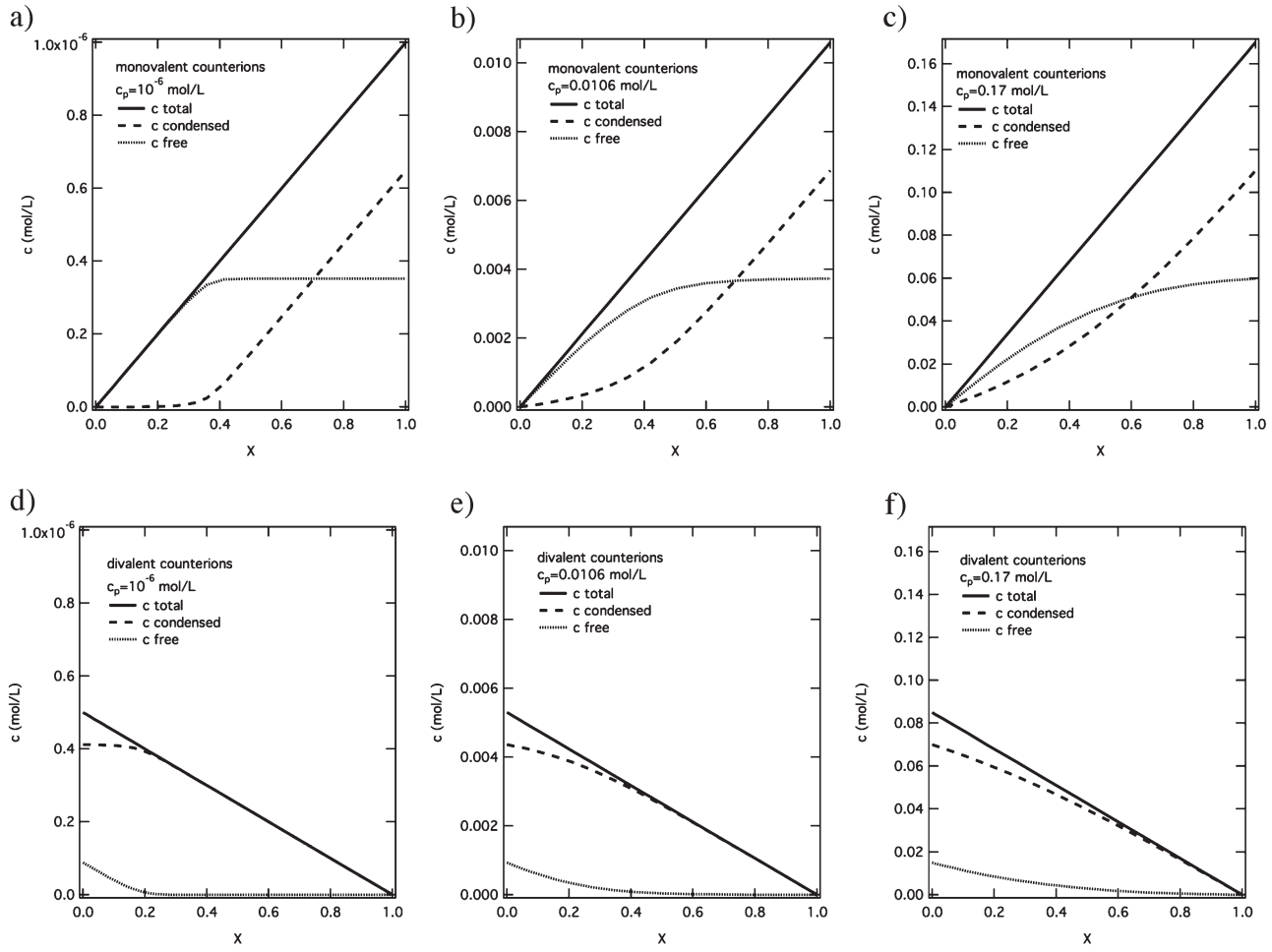

Figure 5. Total, condensed and free counterion concentrations c (mol/L) from the PB equation (upper row, monovalent counterions; lower row, divalent counterions) as a function of X (monovalent/divalent content) for three different polymer concentrations: $c_p = 10^{-6}$ mol/L (a, d); $c_p = 0.0106$ mol/L (b, e); $c_p = 0.17$ mol/L (c, f).

(the free one stays constant), while all divalent counterions are condensed. The effective charge is constant.

In summary, at very low concentration, divalent counterions tend to condense first on the polyions. However, by increasing concentration, the condensed and free counterion repartition slowly departs from this clear-cut variation, and so does the final effective charge fraction. The transition between the previous regimes is gradually smoothed. For example, by comparison with $c_p = 10^{-6}$ mol/L, data for $c_p = 0.17$ mol/L shows that, in the range $0.18 < X < 0.36$:

- For monovalent counterions, the fraction of free counterions is progressively reduced
- At the same time, the fraction of free divalent counterions is not zero anymore.

Such an evolution of the effective charge fraction as a function of X for finite concentrations is related to subtle modifications of counterion distribution within the cell. In the present work, the separation between free and condensed counterions is obtained through the determination of the Manning radii, which requires a close inspection of the integrated radial charge distribution (as a function of $\ln(r)$) to detect a plateau-like evolution. This behavior is highly sensitive to the counterion valence and the polymer concentration. Our results from the PB equation are in accordance with simulations performed on flexible PEL in the presence of pure monovalent, pure divalent or pure trivalent counterions.[48] In this study, authors could also evidence that this plateau-like behavior was less pronounced for higher concentrations and lower valences. It must be mentioned that these authors could demonstrate an increase in the condensed fraction with polymer concentration. In the present work, this cannot be observed due to the procedure applied to separate free from condensed counterions (for pure monovalent or pure divalent counterions, f_{eff} is constant and equal to b/l_B and $b/2l_B$ respectively).

5. DISCUSSION

We have measured the experimental evolution of q^* for different monovalent/divalent contents at distinct concentrations and determined the theoretical evolution of the effective charge fraction f_{eff} in the same conditions. From a qualitative point of view, the measured evolution of q^*, and the predicted variation of the effective charge f_{eff} show a satisfying degree of similarity, and our action seems successful. However, the exact relation between the position q^* and the effective charge fraction of the macroion is not evident to determine.

q versus f,* **Comparison with Literature (Monovalent Counterions).** From an experimental point of view, the

dx.doi.org/10.1021/ma102226v |*Macromolecules* 2011, 44, 3039–3052

evolution of q^* with the polyion charge density, in semidilute solutions in good solvent and for flexible chains, is the starting point and therefore a key point. Surprisingly, experimental studies on this subject are not many. One pioneer work on that field was proposed by Nishida et al.[22] on esterified poly(vinyl alcohol). In this study the position of the scattering peak was measured as a function of the concentration and the polymer charge density. Beside the classical $c_p^{1/2}$ evolution, the most interesting point was the increase of q^* with the chemical charge fraction f up to a crossover value f_{crit}. For higher charge fractions, q^* position was found to be almost constant. This was interpreted as the onset of the counterion condensation leading to a charge renormalization. In the varying regime, q^* was found to vary as $f^{1/3}$, in agreement with other SAXS and SANS results obtained from distinct poly(acrylamide-*co*-acrylic acid) samples.[59] The critical charge density f_{crit} separating the two regimes was also consistent with the condensation threshold determined from MO approach. Another interesting experimental work was also performed by Essafi et al.[23] on poly(acrylamide-*co*-sodium-2-acrylamido-2-methylpropane-sulfonate (AMAMPS). In this approach all different charge densities were above the theoretical condensation threshold. Once more, the main point was the invariance of the position of the scattering peak. Furthermore, a close inspection of the partial scattering function related to the polyions (SANS experiments) evidenced very similar scattering functions indicating analogous chains structure whatever the chemical charge fraction above the condensation threshold. In another set of experiments, the authors tried to determine the effective charge through osmotic pressure measurements.[49] It was concluded that the effective charge was in striking agreement with MO predictions. More recently, the same system has been re-examined using AFM (thin films) and SAXS (bulk) techniques above and below the condensation threshold.[50] The extraction of the correlation length with these two techniques gave identical results: below the condensation threshold, the inverse of the correlation length (thus, proportional to q^*) scales as $f^{2/7}$ within the error bars. For higher charged systems, it becomes constant. The experimental condensation threshold was localized (in between 0.4 and 0.6) close to MO predictions (around 0.36). Similarly, for different rates of partial sulfonation, the scattering of partially sulfonated polystyrene solutions in a solvent good both for sulfonated and non sulfonated sequences (non selective solvent) does not depend on the chemical charge fraction (for f values above 0.36, e.g., above the theoretical condensation threshold close to 0.2).[51]

From these observations, it is clear that q^* is strongly linked to the charge fraction f and thus, is very sensitive to the condensation process: above the condensation threshold the charge density has to be replaced by the effective one f_{eff}.

Yet, predictions of the exact relation between q^* and f, or f_{eff}, in the semidilute regime are diverse. From a theoretical point of view, the structure of the semidilute solutions has been analyzed in term of an "isotropic" transient network by de Gennes.[45] It is then governed by a single characteristic length: the mesh size of the transient network ξ that also represents the screening length of the electrostatic interactions. Thus, the determination of the scattering peak position q^* provides a direct measurement of the correlation length ξ ($q^* = 2\pi/\xi$) and gives insights into the structure of the semidilute solutions.

The scaling approach of de Gennes has been reviewed by Dobrynin, Colby, and Rubinstein.[46] In a good solvent condition, the correlation length ξ can be written as:

$$\xi = f^{-2/7}(l_B/b)^{-1/7}(bc_p)^{-1/2} \quad (17)$$

Here, f is the charge fraction of the PEL. For a given concentration, varying f makes ξ vary,[47] and therefore q^*. This dependence is correlated to the variation of the electrostatic blob size with the charge fraction. We can note that even if experimental measurements agree with the isotropic model, a direct evidence of the existence of electrostatic blobs has never been given.

The scaling model initially applied to weakly charged PEL, for which the charge fraction is the chemical charge fraction of the macroions. However, it is usually assumed also to apply to highly charged PEL. In that case, the macroions are treated as weakly charged PEL with an effective charge fraction f_{eff} taking into account the condensation of part of the counterions. Under this condition, eq 17 becomes

$$\xi = f_{eff}^{-2/7}(l_B/b)^{-1/7}(bc_p)^{-1/2} \quad (18)$$

which gives, for q^*:

$$q^* = 2\pi f_{eff}^{2/7}(l_B/b)^{1/7}(bc_p)^{1/2} \quad (19)$$

Equation 19 perfectly accounts for most of the experimental observations[22,23,50,59] $q^* \propto c_p^{1/2}$ and $q^* \propto f^{\approx 2/7}$. Moreover, as we could show previously,[15] introducing f_{eff} (when necessary) makes this description also account for q^* in many more systems taken from the literature (e.g., different polyions, solvents, chemical charge fractions, above and below the condensation threshold) in the case of monovalent counterions: indeed one obtains a master curve of q^* as a function of $2\pi/\xi$ (instead of the usual concentration c_p). In the scaling approach, the relationship between q^* and the charge fraction f depends on the nature of the interactions between the chains and the solvent. However, if we depart from the case of good solvent conditions, the power law dependence changes with solvent quality: q^* is found to vary as $f^{1/3}$ in Θ solvent and as $f^{1/2}$ under bad solvent condition.[45,46] The bad solvent condition has been the subject of an intense theoretical and experimental research, linked with the expectation of a pearl necklace conformation. This conformation is in agreement with scattering observations of hydrophobic quenched PEL stolutions,[25] and of their polyion conformation.[52] The pearl necklace model also predicts different variations of the power law exponent with the concentration, which we use below.

Mixtures of Counterions and Scaling. Now, our concern is the transposition of such a relation in the case of mixtures of monovalent/divalent counterions. In this case, the chemical charge fraction f (or the degree of sulfonation τ_s) is kept constant but the effective charge is changed by varying the monovalent/divalent content X (and in a less important way, by changing the concentration of the mixture). If the chemical charge fraction f as found in eq 17 was the pertinent parameter, inside the isotropic model, there should be no modification of the position of the electrostatic peak q^* with the monovalent/divalent content, a conclusion obviously not compatible with our observations. This prompts us to replace the charge fraction f, by the effective charge fraction f_{eff} (eq 18) as determined from the resolution of the PB equation. The measurement of q^* thus becomes a quite powerful way to investigate the condensation process in these systems,

provided the nature of the interaction between charges is purely electrostatic. It must be noticed that in our different mixtures, such as $c_p > c_p^*$ (the critical overlap concentration), q^* always scales as $c_p^{1/2}$ in the low concentration regime for pure monovalent counterions, as commonly reported, but *also* for mixtures with divalent. This observation was first reported (at our knowledge) in ref 15. A theoretical approach involving divalent counterions only, predicts the same effect.[53] Both experiments and theory support our scaling approach of data analysis, as long as c_p is concerned.

Coming to the dependence over f_{eff}, an additional difficulty in our case is that the effective charge fraction (as determined from the PB equation) also varies with the concentration c_p. Thus, eq 19 has to be replaced by:

$$q^* = 2\pi(f_{eff}(c_p))^{2/7}(l_B/b)^{1/7}(bc_p)^{1/2} \qquad (20)$$

This c_p dependence provides a clear improvement on our previous study.[15] For a given X value (but $X \neq 0$ and $X \neq 1$), q^* should theoretically vary with the concentration through the effective charge dependence $f_{eff}(c_p)$. Because of the related weak exponent of the power law (2/7), this effect should lead to very subtle—while measurable—variations and could introduce small deviations to the $c_p^{1/2}$ classical behavior. Note that due to our effective charge determination procedure, f_{eff} does not depend on c_p for pure monovalent ($X = 1$), and pure divalent ($X = 0$), while Monte Carlo simulations show a slight variation in practice (which is expectable).

We will now compare systematically below the variation of q^* as a function of X with the calculated ones using the scaling $q^*(f_{eff})$ and our two determinations of f_{eff}. This is done in Figure 3 for the effective charge fraction evaluated from MO approach (using eq 19) and from the PB equation (using eq 20). In these plots, the vertical position of the theoretical curves is adjusted to the experimental values obtained for $X = 1$. Since the experimental and theoretical evolutions are in accordance with $q^* \propto c_p^{1/2}$ for $X = 1$, this is equivalent to consider a single global prefactor for the whole set of data (which, in theory should be closed to $2\pi(l_B/b)b^{1/2}$).

Comparison with the Manning−Oosawa Approach. The first comparison is with computations of the effective charge in the classical MO approach. The theoretical evolution of q^* as a function of X can be divided in three portions which reproduce the evolution of the effective charge (Figure 3, dashed lines). Between $X = 0$ and $X = b/2\,l_B$, as well as $X = b/l_B$ and $X = 1$, we get a plateau since the effective charge is constant. In between $X = b/2\,l_B$, and $X = b/l_B$, q^* varies as $X^{2/7}$.

Obviously, the theoretical plateau for $X < b/2\,l_B$ is never observed experimentally. Above $b/2\,l_B$, the general theoretical trend is only reproduced for the two lowest concentrations (c_p = 0.0106 and 0.0212 mol/L). However, even for these two concentrations, a close examination already indicates a decrease in the experimental q^* values below $X = 0.6$ and thus a deviation from the theoretical plateau. This deviation is more and more pronounced as c_p is increased and the plateau disappears for $c_p \geq$ 0.0425 mol/L.

While the MO approach roughly describes the low concentration regime above $X = b/2\,l_B$ (as already mentioned in ref 15), it cannot explain the deviations from the theoretical plateau at high X, as well as the absence of any plateau below $X = b/2\,l_B$.

Comparison with the Poisson−Boltzmann Approach. The continuous increase of q^* with X observed from SAXS data, can be obtained solving the PB equation (Figure 3, solid lines).

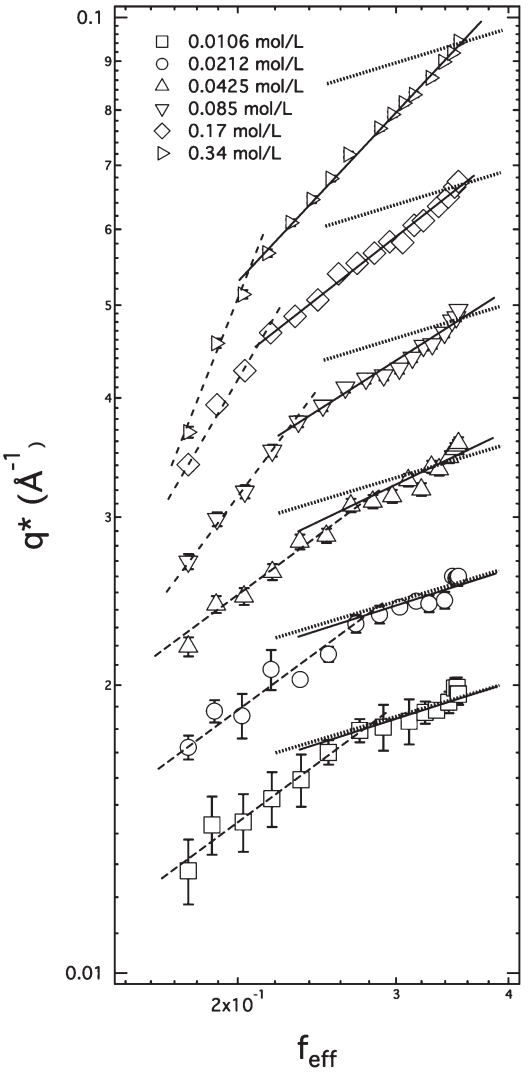

Figure 6. Evolution of experimental q^* values as a function of the theoretical effective charge f_{eff} determined from the resolution of the PB equation. Long dashed lines represent power laws for small X values (regime A). Lines represent power laws for large X values (regime B). Short dashed lines correspond to the theoretical law $q^* \propto f_{eff}^{2/7}$. Power law exponents are listed in Table 2.

For the two lowest concentrations, the variation of q^* with X is nicely predicted for $X > 0.25$. In particular, the deviation from the high X theoretical plateau (from MO approach as discussed above) is fairly reproduced. For higher concentrations, the domain of agreement starts to reduce down to the highest X values only. The variation of the effective charge with c_p is not large enough to properly explain the experimental behavior. The general tendency is however correctly rendered.

For $X < 0.25$, no plateau is predicted. This is in contrast with the MO approach, and closer to data. But the theoretical variation of q^* is much weaker than the experimental one: there is no quantitative agreement in this region even at the two lowest concentrations. However, low X corresponds to a majority of divalent Ca^{2+} counterions and their local correlations are not accounted for.

q versus f_{eff}.* The partial failure of comparison of experimental $q^*(X)$ with calculated values obtained through the scaling of $q^*(f_{eff})$, can be due either to a wrong scaling assumption or to a

Table 2. Power Law Exponents and Crossover Effective Charge Fractions[b]

c_p (mol/L)	$f_{\text{eff crossover}}$	α_A (regime A)	α_B (regime B)
0.0106	0.27 ± 0.02	$\alpha_A = 0.70 \pm 0.20$	$\alpha_B = 0.30 \pm 0.05$ (2/7 = 0.286)
0.0212	0.28 ± 0.02	$\alpha_A = 0.70 \pm 0.20$	$\alpha_B = 0.30 \pm 0.05$
0.0425	0.27 ± 0.02	$\alpha_A = 0.70 \pm 0.20$	$\alpha_B = 0.45 \pm 0.05$
0.085	0.23 ± 0.01	$\alpha_A = 1.18 \pm 0.05$	$\alpha_B = 0.60 \pm 0.05$
0.17	0.215 ± 0.010	$\alpha_A = 1.44 \pm 0.10$	$\alpha_B = 0.73 \pm 0.05$
0.34	0.205 ± 0.010	$\alpha_A = 2.35 \pm 0.10$	$\alpha_B = 1.00 \pm 0.05$

[b] Crossover effective charge fraction $f_{eff\ crosssover}$, and power law exponents α_A and α_B in regime A and regime B. Regime A and regime B correspond to smaller and higher X values, respectively.

wrong estimate of f_{eff}. Though this will not suffice to distinguish between these two origins, focusing on scaling of experimental q^* versus theoretical f_{eff} calculated from the PB approach reveals interesting behaviors. Figure 6 is plotted in log−log scale to evidence apparent power laws. We see that the function q^* (f_{eff}) can be roughly described, for each concentration, by two successive power law regimes, noted A for low f_{eff}, and B for large f_{eff}. The crossover between A and B occurs at a charge fraction $f_{eff\ crossover}$. For the two lowest concentrations $f_{eff\ crossover} \sim 0.27$ and separates a large X regime B close to the theoretical variation (exponent $\alpha_B = 0.30 \pm 0.05$ close to 2/7), from a low X regime A with exponent $\alpha_A = 0.70 \pm 0.20$. This also applies, to a lower extend, to $c_p = 0.0425$ mol/L, though α starts to increase in regime B ($\alpha_B = 0.45 \pm 0.05$). If c_p is increased, $f_{eff\ crossover}$ reduces, while both α_A and α_B increase, as summarized in Table 2, so that the theoretical $f_{\text{eff}}^{2/7}$ line is not followed at all.

The evolution of q^* could also suggest a third regime at the highest effective charges, thus dividing regime B into two different parts. With such a distinction, the intermediate regime corresponding to a power law exponent ∼0.30 can then be extended up to $c_p = 0.085$ mol/L. However, its domain of existence is reduced as the concentration is increased (it finally disappears for $c_p \geq 0.17$ mol/L). In the following, we will not consider this description and will only focus on the two regimes picture (A and B).

Therefore, if we consider the lowest concentrations, we clearly see that for $f_{\text{eff}} > 0.27$, the evolution of q^* is compatible with the scaling law $q^* \propto f_{\text{eff}}^{2/7}$ as predicted in eq 20 ($\alpha = 0.3 \sim 0.285 = 2/7$). This means that for the low concentration regime, and effective charge fraction larger than 0.27 ($X > 0.30$, i.e. more than 46% of monovalent counterions), the variation of the structure of the solution can be fully understood solely on the basis of an effective charge modification: the scaling law initially predicted for weakly charged PEL (and experimentally found to be close to 1/3 in ref 22 and to 2/7 in ref 50) also applies for highly charged polyions and mixtures of monovalent and divalent counterions if we replace the chemical charge fraction by the effective one. Mixing counterion valences thus provides a different way to tune the effective charge fraction without modification of the chemical sequence of the polyions.

However, the presence of divalent counterions reduces the validity range of this assumption: actually both the divalent counterion ratio and the concentration (therefore the divalent counterion concentration) must remain small enough. This conclusion appears close to the results of ref 33. In this study, authors compare theoretical osmotic coefficients derived from PB calculations, modified PB calculations, and Monte Carlo simulations. If all of their calculations capture the main features of experimental measurements, it is however demonstrated that for large divalent contents (small X values in our study), simple PB calculations overestimate the osmotic coefficients, and thus underestimate the counterion condensation, as we do here also at small X. This would imply that here the estimate of f_{eff} is wrong, not necessarily the scaling. But other reasons may exist.

Physical Origins of Discrepancy. These discrepancies at large divalent content are likely due to the fact that ion−ion correlations are neglected in the PB equation approach. But more precisely it is also important, as mentioned in ref 33, to keep in mind that these different models completely ignore the details on a molecular scale, details that could be very important in the case of specific interactions (which we ignored until now). Let us remember the core of the isotropic model: the chain is modeled as an assembly of electrostatic blobs. The relation between ξ and f_{eff} in semidilute regime (eq 17 to 20) thus implies the internal structure within the blob, like a self-avoiding random walk in good solvent conditions giving $\xi \propto f^{-2/7}$ (or $\xi \propto f_{\text{eff}}^{-2/7}$), whereas a random walk in Θ solvent, $\xi \propto f^{-1/3}$.

These interactions between chain segments make vary the electrostatic blob size and by consequence the effective contour length[22] and the linear density. Thus, any other phenomenon (distinct from charge fraction or blob statistics) able to change the local structure or the effective contour length, may also induce q^* variations. Naturally, we must also keep in mind the effect of charge fraction: different recent theoretical approaches, in the case of rigid polyion and for multivalent counterions, predict an effective charge fraction much lower than MO model.[54] But we will focus now on conformational aspects.

Chain Conformation Aspects. Along this line of thought about conformation, an additional point to discuss is the relation with hydrophobicity via the pearl necklace model.[55] In the effective charge range $0 < f_{\text{eff}} < 0.27$, we have seen just above an apparent power law with exponent $\alpha_A \sim 0.70 \pm 0.20$ for c_p = 0.0106, 0.212, and 0.425 mol/L (see long dashed lines in Figure 6). This is far from 2/7 = 0.285 or 1/3 = 0.33 expected in good or Θ solvent, but close to the one encountered for PEL in poor solvent. For these conditions, the pearl-necklace model for the polyion conformation predicts more than one concentration regime above c_p^*. In a first "low concentration" regime, called string controlled regime, q^* varies as $c_p^{1/2}$ and $f^{1/2}$. For higher concentrations, we enter in the bead controlled regime, and q^* varies as $c_p^{1/3}$ and $f^{2/3}$. If we consider that the charge fraction can be replaced by the effective one f_{eff}, we see that our low concentration observations (for which q^* varies as $c_p^{1/2}$) could be compatible with the string-controlled regime ($q^* \sim f^{0.7\pm0.2}$ to compare to $f^{1/2}$). In other words, the origin of a high exponent α_A could be related to some hydrophobic character of the macroions, as in the case of partially sulfonated PSS. This interpretation was indirectly invoked in ref 56, but it is not

supported by pyrene fluorescence measurements performed formerly in our group,[15] which do not indicate the existence of any hydrophobic zones. In practice, accurate comparisons can be done using form factor measurements, achieved using SANS. In the case of hydrophobicity due to uncomplete sulfonation of the polystyrene, the form factor is well described by a pearl necklace conformation.[52] If reducing the effective charge of PSS by increasing the divalent counterion ratio were equivalent to reducing the sulfonation rate, this effect should be maximal for $X = 0$ (CaPSS). The possibility of necklace globule formation, not due to hydrophobicity but only to the counterions condensation has also been predicted recently for flexible macroions in good solvent conditions.[58] In practice, form factor measurements realized for pure CaPSS[57] does reveal a change of conformation, but it is different from the pearl necklace one: the conformation is also more compact, akin to a shrinking of the chain at short scales, shortening the contour length and increasing the linear density, while the wormlike conformation is kept at large scale.[57] This is accompanied by a shift of the correlation peak to smaller q values (as in our measurements), in agreement with the transient network picture. The mechanism of such a local shrink is still unclear but could be related to local bridging—probably with a short lifetime—of the chain by divalent counterions. In summary, we can conclude that these form factors clearly suggest that the deviation in $q^*(X \text{ or } f_{\text{eff}})$ which we observe is associated, at least in part, to a change of conformation toward a more compact one.

Finally, for higher concentrations (c_p = 0.085, 0.17, and 0.34 mol/L) and high divalent contents, deviations from the $q^* \propto {c_p}^{1/2}$ law appear (Figure 2, see also ref 15). This behavior is consistent with eq 20 since the effective charge fraction is reduced with increasing concentration. However, as can be found from Figure 3, the calculated deviations are definitively too small to reproduce the data, at least as determined from the PB equation. Like for the smallest concentration, two power law regimes are still visible on $q^*(f_{\text{eff}})$ in Figure 6. We can notice that in this concentration range, electrostatic interactions are more screened than for the lowest concentration. Thus, local modifications of the polyion structure become easier and easier. Form factor measurements in this concentration range should certainly be very useful to understand these particular effects. This would enable us to assess the level of influence of the conformational effects in the observed deviations, compared with intercounterions correlations. Note that even in the regime where scaling is obeyed, we should observe an evolution of the form factor, since the electrostatic blob size varies.

Final Summary. In this work, the use of the cylindrical cell model is an attempt to determine the effective charge fraction, a very important parameter for explaining the scattering behavior of PEL with mixed monovalent and divalent counterions. We combined it with the isotropic model approach. The result is 2-fold:

- For high concentration, as well as for large divalent counterion content, this approach fails. There are currently very little theories, or simulations dealing with monovalent/divalent mixtures under salt free conditions in the case of flexible PEL. Most of them only focus on monovalent or divalent counterions, or only introduce divalent ions through added salt, and most often only consider rigid PEL. We hope that these experiments and their rather complete set of results will help in theory improvement. Conformation measurements should also be accounted for a better understanding of the way multivalent counterions act on the chain. We do not know yet the level of influence of such conformational effects
- For low concentrations, providing that the divalent counterion content is not too high, this approach gives reasonable effective charge values and allows a reasonable understanding of the main experimental scattering features. Thus, in this range, the cylindrical cell model is useful, in expectation of a more adequate approach.

6. SUMMARY AND CONCLUSION

In this article, we studied the structure of salt free semidilute solutions of flexible PEL containing monovalent and divalent counterions through SAXS. This work is a continuation of a previous study in which only a limited number of mixtures were investigated. We have chosen to work on NaPSS/CaPSS mixed solution for which interactions other than electrostatic are not expected to play a key role. Polyions were highly charged and carried almost one charge per monomer. Their high chemical charge fraction is responsible for a counterion condensation process, which leads to a charge renormalization.

SAXS patterns show a scattering peak at a position q^* which depends on the concentration and the monovalent/divalent mixture content. In the low concentration range, each mixture (including solution with pure divalent counterions) shows an evolution of the type $q^* \propto {c_p}^{1/2}$. Within the isotropic model, the position of the PEL peak is related to the correlation length ξ, and therefore, to the local structure of the polyions as well as to their effective charge fraction. Thus, measuring q^* as a function of the concentration and of the monovalent/divalent content provides a way to understand the structure of the solution and to get insight into the complex condensation phenomena.

The effective charge fraction has been computed from the PB equation within the cylindrical cell model for several mixtures. It exhibits a clear dependence on the monovalent/divalent content. In these solutions, the divalent counterions condense first. Depending on the monovalent/divalent content, monovalent and divalent counterions can be free or condensed along the macroions. This scenario also shows a complex concentration dependence and MO predictions can only be retrieved for infinitely diluted samples. Mixtures can also be seen as a way to tune the effective charge fraction without changing the chemical nature of the polyions.

The q^* values have been analyzed within the isotropic model including a calculated effective charge fraction from the PB equation. This model captures the main features of the experimental data and can even be considered as quantitative for very low concentrations provided the divalent content is not too high. The evolution of q^* versus the calculated effective charge fraction f_{eff} seems to evidence two power law regimes for the whole set of concentrations. Main results can be summarized as follows:

- In the low concentration regime, providing that the divalent content is not too large, the position of the PEL peak q^* is compatible with the scaling approach. In particular, the power law exponent in the relation $q^* \propto {f_{\text{eff}}}^{\alpha}$ is found to be very close to 2/7, a typical exponent encountered for PEL in good solvent conditions. Thus, a change in the position of the PEL peak can be understood on the basis of a simple effective charge fraction variation. The structure of the solution, and probably of the chain, is then very similar to that of a weakly charged polyion if we replace the chemical charge fraction by the effective one

- Still in the low concentration regime, but when the divalent content is increased, deviations from the previous description occur. New effects start to appear and are not taken into account in the PB equation. These effects are in agreement with a contraction of the chain leading to a decrease of the total contour length and finally lead to an additional decrease in the position of the PEL peak, as seen before by Dubois et al.[57] for pure CaPSS. This could be due to bridging phenomena from the divalent counterions. But we ignore the level of influence of the conformational effects in the observed deviations, with respect to purely intercounterion correlations
- In the high concentration range, scaling exponents in both regimes are not quantitatively consistent with any theoretical predictions. It is clear that form factor measurements using neutron scattering would certainly improve our understanding in this concentration range. Such a study will be presented in a forthcoming paper.

■ ASSOCIATED CONTENT

Supporting Information. Scattering curves measured for different X values at different concentrations. This material is available free of charge via the Internet at http://pubs.acs.org.

■ AUTHOR INFORMATION

Corresponding Author

*Telephone: +33 3 88 41 40 96. Fax: +33 03 88 41 40 99. E-mail: jerome.combet@ics-cnrs.unistra.fr.

Present Addresses

†Institut Laue Langevin, BP 156, 6 rue Jules Horowitz 38042 Grenoble cedex 9, France. E-mail: jerome.combet@ill.fr.

■ ACKNOWLEDGMENT

We warmly thank the staff of Dubble and D2AM beamlines at ESRF for efficient help during these experiments, as well as Wim Bras for his lively support. The ESRF is acknowledged for beam time allocation. We also thank our colleagues of the synthesis groups of ICS-Strasbourg, in particular Franz Isel, who conducted the synthesis of NaPSS and CaPSS.

■ REFERENCES

(1) Hara, M., Ed. *Polyelectrolytes: Science and Technology*; Marcel Dekker; New York, 1993.

(2) Schmitz, K. S. *Macroions in Solution and Colloidal Suspensions*; VCH: New York, 1993.

(3) Förster, S.; Schmidt, M. *Adv. Polym. Sci.* **1995**, *120*, 51.

(4) Barrat, J.-L.; Joanny, J.-F. *Adv. Chem. Phys.* **1996**, *94*, 1.

(5) Radeva, T., Ed. *Physical Chemistry of Polyelectrolytes*; Marcel Dekker; New York, 2001.

(6) Holm, C., Kekicheff, P., Podgornik, R., Eds. *Electrostatic Effects in Soft Matter and Biophysics*; Vol. 46 of NATO Science Series II-Mathematics, Physics and Chemistry; Kluwer Academic Press; Dordrecht, The Netherlands, 2001.

(7) Dobrynin, A. V.; Rubinstein, M. *Prog. Polym. Sci.* **2005**, *30*, 1049.

(8) Manning, G.S. J. *Chem. Phys.* **1969**, *51*, 954.

(9) Oosawa, F. *Biopolymers* **1968**, *6*, 134.

(10) Schweins, R.; Huber, K. *Eur. Phys. J. E* **2001**, *5*, 117. Schweins, R.; Goerigk, G.; Huber, K. *Eur. Phys. J. E* **2006**, *21*, 99.

(11) Axelos, M. A.; Mestdagh, M. M.; François, J. *Macromolecules* **1994**, *27*, 6594. Heitz, C. Thesis, Université Louis Pasteur de Strasbourg: Strasbourg, France, 1996; François, J.; Heitz, C.; Mestdagh, M. M. *Polymer* **1997**, *38*, 5321. Heitz, C.; François, J. *Polymer* **1999**, *40*, 3331.

(12) Stevens, M.-J. *Phys. Rev. Lett.* **1999**, *82*, 101.

(13) Sabbagh, I.; Delsanti, M.; Lesieur, P. *Eur. Phys. J. B* **1999**, *12*, 253. Sabbagh, I., Thesis, Université Paris VII: Paris, France, 1997.

(14) Sabbagh, I.; Delsanti, M. *Eur. Phys. J. E* **2000**, *1*, 75. Drifford, M.; Delsanti, M. In *Physical Chemistry of Polyelectrolytes*; Radeva, T., Ed.; Marcel Dekker; New York, 2001, Chapter 4, pp 135−161.

(15) Combet, J.; Isel, F.; Rawiso, M.; Boué, F. *Macromolecules* **2005**, *38*, 7456.

(16) Nierlich, M.; Williams, C. E.; Boué, F.; Cotton, J.-P.; Daoud, M.; Farnoux, B.; Jannink, G.; Picot, C.; Moan, M.; Wolf, C.; Rinaudo, M.; de Gennes, P.-G. *J. Phys. (Fr.)* **1979**, *40*, 701.

(17) Prabhu, V. M. *Curr. Opin. Colloid Interface Sci.* **2005**, *10*, 2.

(18) Prabhu, V. M.; Amis, E. J.; Bossev, D. P.; Rosov, N. *J. Chem. Phys.* **2004**, *121*, 4424.

(19) van der Maarel, J. R. C.; Groot, L. C. A.; Hollander, J. G.; Jesse, W.; Kuil, M. E.; Leyte, J. C.; Leyte-Zuiderweg, L. H.; Mandel, M.; Cotton, J. P.; Jannink, G.; Lapp, A.; Farago, B. *Macromolecules* **1993**, *26*, 7295.

(20) Bhuiyan, L. B.; Outhwaite, C. W.; van der Maarel, J. R. C. *Physica A* **1996**, *231*, 295.

(21) Kassapidou, K.; Jesse, W.; Kuil, M. E.; Lapp, A.; Egelhaaf, S.; van der Maarel, J. R. C. *Macromolecules* **1997**, *30*, 2671.

(22) Nishida, K.; Kaji, K.; Kanaya, T. *Macromolecules* **1995**, *28*, 2472.

(23) Essafi, W.; Lafuma, F.; Williams, C. E. *Eur. Phys. J. B* **1999**, *9*, 261.

(24) Makowski, H. S.; Lundberg, R. D.; Singhaln, G. S. US Patent 3,870,841, 1975, to Exxon Research and Engineering Company.

(25) Essafi, W.; Lafuma, F.; Williams, C. E. In *Macroion characterization from dilute solutions to complex fluids*; Schmitz, K. S., Ed.; ACS Symposium Series 548; American Chemical Society: Washington, DC, 1994, Chapter 21, pp 278−286.

(26) Essafi, W. Thesis, Université Paris VI: Paris, France, 1996.

(27) Heinrich, M. Thesis, Université Louis Pasteur: Strasbourg, France, 1998.

(28) Tondre, C.; Zana, R. *J. Phys. Chem.* **1972**, *76*, 3451.

(29) Millero, F. J. In *Water and Aqueous Solutions*; Horne, R. A., Ed.; Wiley-Interscience: New York, 1972, Chapter 13.

(30) Skerjanc, J.; Dolar, D. *J. Chem. Phys.* **1989**, *91*, 6290.

(31) Dolar, D.; Peterlin, A. *J. Chem. Phys.* **1969**, *50*, 3011.

(32) Das, T.; Bratko, D.; Bhuiyan, L. B.; Outhwaite, C. W. *J. Phys. Chem.* **1995**, *99*, 410.

(33) Das, T.; Bratko, D.; Bhuiyan, L. B.; Outhwaiten, C. W. *J. Chem. Phys.* **1997**, *107*, 9197.

(34) Manning, G. S. In *Polyelectrolytes*; Sélégny, E., Ed.; Reidel Publishing Company; Dordrecht, The Netherlands, 1974; pp 9−37.

(35) Dolar, D. In *Polyelectrolytes*; Sélégny, E. (Ed.); Reidel Publishing Company; Dordrecht, The Netherlands, 1974; pp 97−113.

(36) Fuoss, R. M.; Katchalsky, A.; Lifson, S. *Proc. Natl. Acad. Sci. U S A.* **1951**, *37*, 579.

(37) Alfrey, T.; Berg, P. W.; Morawetz, H. *J. Polym. Sci.* **1951**, *7*, 543.

(38) Mandel, M. *J. Phys. Chem.* **1992**, *96*, 3934.

(39) Guilleaume, B.; Blaul, J.; Wittemann, M.; Rehahn, M.; Ballauff, M. *J. Phys.: Condens. Matter* **2000**, *12*, A425.

(40) Ballauff, M.; Blaul, J.; Guilleaume, B.; Rehahn, M.; Traser, S.; Wittemann, M.; Wittmeyer, P. *Macromol. Symp.* **2004**, *211*, 1.

(41) Liao, Q.; Dobrynin, A. V.; Rubinstein, M. *Macromolecules* **2003**, *36*, 3399.

(42) Deserno, M.; Holm, C.; May, S. *Macromolecules* **2000**, *33*, 199. Deserno, M. Thesis, Johannes Gutenberg-University: Mainz, Germany, 2000.

(43) Belloni, L.; Drifford, M.; Turq, P. *Chem. Phys.* **1984**, *83*, 147. Belloni, L. *Colloids Surf.* **1998**, *A140*, 227.

(44) Kaji, K.; Urakawa, H.; Kanaya, T.; Kitamaru, R. *J. Phys. (Fr.)* **1988**, *49*, 993.

(45) de Gennes, P.-G.; Pincus, P.; Velasco, R. M.; Brochard, F. *J. Phys. (Fr.)* **1976**, *37*, 1461.

(46) Dobrynin, A. V.; Colby, R. H.; Rubinstein, M. *Macromolecules* **1995**, *28*, 1859.
(47) Pfeuty, P. *J. Phys., Colloq.* **1978**, *C2*, 149.
(48) Holm, C.; Kremer, K. in Proceedings of Yamada Conference Polyelectrolytes; Yamada Science Foundation: Osaka, Japan, 1999; p 27.
(49) Essafi, W.; Lafuma, F.; Baigl, D.; Williams, C. E. *Europhys. Lett.* **2005**, *71*, 938.
(50) Qu, D.; Pedersen, J. S.; Garnier, S.; Laschewsky, A.; Möhwald, H.; v. Klizing, R. *Macromolecules* **2006**, *39*, 7364.
(51) Essafi, W.; Spiteri, M. N.; Williams, C. E.; Boué, F. *Macromolecules* **2009**, *42*, 9568.
(52) Spiteri, M. N.; Williams, C. E.; Boué, F. *Macromolecules* **2007**, *40*, 6679.
(53) Chang, R.; Yethira, A. *J. Chem. Phys.* **2003**, *118*, 11315.
(54) Nyquist, R. M.; Ha, B. Y.; Liu, A. J. *Macromolecules* **1999**, *32*, 3481.
(55) Dobrynin, V.; Rubinstein, M. *Macromolecules* **1999**, *32*, 915.
(56) Zhang, Y.; Douglas, J. F.; Ermi, B. D.; Amis, E. J. *J. Chem. Phys.* **2001**, *114*, 3299.
(57) Dubois, E.; Boué, F. *Macromolecules* **2001**, *34*, 3684.
(58) Jeon, J.; Dobrynin, A. V. *Macromolecules* **2007**, *40*, 7695.
(59) El Brahmi, K. Thesis, Université Louis Pasteur de Strasbourg: Strasbourg, France, 1991
(60) Netz, R. R.; Orland, H. *Eur. Phys. J. E.* **2003**, *11*, 301.